Fidelity of measurement-based quantum computation in a bosonic environment

Jian Wang,[1] Ding Zhong,[1] Liangzhu Mu,[1,*] and Heng Fan[2,†]
[1]*Peking University, Beijing 100871, China*
[2]*Institute of Physics, Chinese Academy of Sciences, Beijing 100190, China*
(Received 15 April 2014; revised manuscript received 22 September 2014; published 6 November 2014)

We investigate the fidelity of measurement-based quantum computation (MBQC) when it is coupled with a boson environment, by measuring the cluster-state fidelity and gate fidelity. Two schemes of cluster-state preparation are studied. In the controlled-Z (CZ) creation scheme, cluster states are prepared by entangling all qubits in $|+\rangle$ state with CZ gates at all neighboring sites. The fidelity shows an oscillation pattern over time. The influence of the environmental temperature is evaluated, and suggestions are given to enhance the performance of MBQCs realized in this way. In the Hamiltonian creation scheme, cluster states are made by cooling a system with cluster Hamiltonians, of which the ground states are cluster states. A fidelity sudden-drop phenomenon is discovered. When the coupling is below a threshold, MBQC systems are highly robust against the noise. Our main environmental model is one with a single collective bosonic mode.

DOI: 10.1103/PhysRevA.90.052306 PACS number(s): 03.67.Pp, 03.67.Lx

I. INTRODUCTION

Measurement-based quantum computation (MBQC) is a widely accepted scheme for quantum computation [1–3]. Instead of designing complicated quantum gates to manipulate qubits, MBQC is implemented by executing a sequence of single-qubit measurements on cluster states consisting of a group of highly entangled qubits. As a result, one great difficulty lies in the cluster-state preparation.

There are various proposals for preparing cluster states. In optics, a fusion operation to bind small cluster states into a larger cluster state is used [4,5]. For quantum dots, there is another method [6]. In Ref. [2], Raussendorf *et al.* pointed out two general ways to prepare cluster states. The first is to prepare all qubits in $|+\rangle$ state and entangle them into a cluster state by implementing controlled-Z (CZ) gates on all neighboring sites. The second is to design a so-called cluster Hamiltonian, of which the ground state is a cluster state, and then cool down the system to obtain an approximate cluster state. The idea of a cluster Hamiltonian has been further explored. For example, one can encode four physical qubits into one logical qubit to achieve an experimentally realizable cluster Hamiltonian [7]. It has also been shown that topologically protected MBQC can reduce thermal fluctuations [8] in the Hamiltonian-created cluster state. Experiments on optical systems have been performed to demonstrate various quantum algorithms and protocols using the MBQC scheme. In 2005, Walther *et al.* reported a demonstrative experiment on four-qubit cluster states [9]. In 2007, Grover's search algorithm for four qubits was reported [10]. Also, Deutsch's algorithm was realized by MBQCs on a four-qubit optical system [11]. Remarkably, in the same year, a six-photon cluster state was successfully entangled by Pan's group [12]. The one-way MBQC scheme has even been used to test the quantum version of the prisoner's dilemma [13]. A four-photon cluster state with a very high fidelity is demonstrated in Ref. [14]. The realization of MBQCs beyond the cluster state has also been reported [15].

Unfortunately, cluster states, as a highly entangled system, are fragile to decoherence. It is thus important to analyze the noise to ensure that the computation on a cluster state is reliable. Some works have been done on this topic. In 2006, a method was proposed for checking the fidelity of a four-qubit cluster state experimentally [16]. The entanglement sudden death phenomenon [17], which may affect the fidelity of cluster states, has also been studied [18]. Recently, Fujii *et al.* studied the error appearing in Hamiltonian-created cluster states when the temperature is nonzero [19]. They discovered that the fidelity changes suddenly at a certain threshold temperature.

In this paper, we analyze the performance of the MBQC system when coupled with a boson environment (Fig. 1). The cluster-state fidelity and four kinds of gate fidelity are measured, and the gate fidelity is studied in detail.

Due to the threshold theorem of fault-tolerant quantum computation, if the error in individual quantum gates is below a certain threshold, quantum computation on a large scale can be achieved as well [20]. As a result, our analysis works to protect MBQC systems with arbitrary scales.

The boson environment has long been an issue of concern in various fields [21]. More importantly, the boson environment, which is the noise caused by harmonic oscillators, actually describes a wide range of weak noises. Thus, this noise model is generic to many quantum computation cases.

A large cluster state can be prepared bit by bit. Therefore, a strategy against noise is to prepare a portion of a cluster state right before it is measured. In this paper, we assume that the cluster state for an individual gate operation is prepared at one time. With individual gate fidelities being analyzed, the fidelity of the whole MBQC can then be studied by the scheme of fault-tolerant quantum computation.

Two preparation schemes for the cluster state are evaluated. The first scheme was proposed by Briegel and Raussendorf [22]. In this scheme, cluster states are prepared by entangling all qubits previously in the $|+\rangle$ state with CZ gates on neighboring sites. The second scheme was later proposed by Raussendorf [2], where cluster states are made by cooling a system with cluster Hamiltonians, and the cluster states are

*muliangzhu@pku.edu.cn
†hfan@iphy.ac.cn

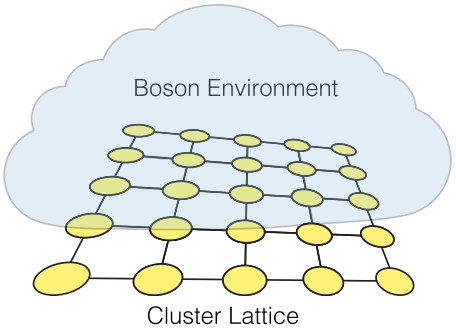

FIG. 1. (Color online) A cluster state coupled with a boson environment.

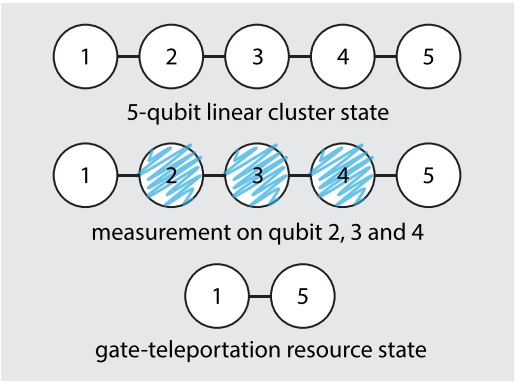

FIG. 2. (Color online) Using a five-qubit linear cluster state to produce the gate teleportation resource state for Z rotation.

the ground states. Both preparations are significant and widely applicable. However, since the two preparation schemes are quite different, it may not be meaningful to compare the fidelity between them.

This paper is organized as follows. In Sec. II, we introduce gate fidelity. In Sec. III, we analyze how the coupling of a boson environment affects the cluster state entangled by CZ gates. We first solve the pure phase noise case exactly and analyze it in detail. Suggestions are given for minimizing the damage caused by the coupling. Then we consider both phase noise and amplitude noise, which is a more general case. We solve this problem numerically. In Sec. IV, we analyze the influence of a boson environment on the cluster Hamiltonian situation, with both phase and amplitude noise considered. We also discover a threshold coupling coefficient at which the fidelity drops dramatically. Section V presents the discussion. We address the difference between the gate fidelity and the corresponding cluster-state fidelity. The collective character of our noise model is also discussed. We present our conclusions in Sec. VI.

II. INTRODUCTION TO THE FIDELITY FOR GATE OPERATIONS

The fidelity for a cluster state [2] is defined straightforwardly,

$$F = \mathrm{Tr}(|\Psi_C\rangle\langle\Psi_C|\rho), \tag{1}$$

where $|\Psi_C\rangle$ is a perfect cluster state, and ρ is the state being judged. The form and utility of a cluster state $|\Psi_C\rangle$ are reported in Ref. [2].

However, we are often more concerned with how well a gate operation is implemented by an MBQC system, and the cluster-state fidelity fails to answer this question. It is thus necessary to define the fidelity for gate operations. A good definition employs a process called gate teleportation.

The basic idea of gate teleportation is simple: if you apply some unitary operations to an EPR pair and use the pair to teleport a qubit, rather than getting the original information from the transported qubit, you will receive transformed information. By applying the proper gate to the EPR pair, we can get the transported qubit transformed by a desired unitary operator. For example, if you would like to have a qubit with Hadamard gate applied, rather than teleporting it by a regular EPR pair $(|00\rangle + |11\rangle)$, we teleport it by $(I \otimes H)(|00\rangle + |11\rangle)$. Readers may refer to the original paper on gate teleportation [23] to get a full understanding.

It turns out that a cluster state can be used to prepare resource states for gate teleportation by implementing a one-way scheme. This fact offers a way to define gate fidelity [19,24]. We take a Z-rotation gate as an example to illustrate this process. The Z-rotation operation is defined as

$$R_\theta = \begin{pmatrix} e^{i\frac{\theta}{2}} & 0 \\ 0 & e^{-i\frac{\theta}{2}} \end{pmatrix}, \tag{2}$$

and the resource state for it is $R_{\theta,2}(|00\rangle + |11\rangle)_{12}$.

We prepare the resource state from a five-qubit linear cluster state (Fig. 2). The resource state is prepared by a similar measurement sequence to implement a Z-rotation gate in an MBQC system. First, measure qubit 2 on the basis of the Pauli X operator. The resulting state is

$$|\pm\rangle_2 X_1^{m_2}(|00\rangle + |11\rangle Z_4)_{13}(|0\rangle + |1\rangle Z_5)_4(|0\rangle + |1\rangle)_5. \tag{3}$$

When the outcome of the measurement is $|\psi\rangle_2 = |+\rangle, m_2 = 0$; when the outcome is $|\psi\rangle_2 = |-\rangle, m_2 = 1$. Then we measure qubit 3 on the basis of

$$\cos\tilde{\theta}X + \sin\tilde{\theta}Y = e^{-i\frac{\tilde{\theta}}{2}Z}Xe^{i\frac{\tilde{\theta}}{2}Z}. \tag{4}$$

Here, $\tilde{\theta} = \pm\theta$ when $|\psi\rangle_2 = |\pm\rangle$, respectively. The eigenstate of this operator is

$$|\varphi_+\rangle = \cos\frac{\tilde{\theta}}{2}|+\rangle - i\sin\frac{\tilde{\theta}}{2}|-\rangle, \tag{5}$$

$$|\varphi_-\rangle = \cos\frac{\tilde{\theta}}{2}|-\rangle - i\sin\frac{\tilde{\theta}}{2}|+\rangle. \tag{6}$$

After the measurement of qubit 3, the system becomes

$$\begin{aligned} &|\varphi_\pm\rangle_3 X_1^{m_2} Z_1{}^{m_3}(|0\rangle e^{i\frac{\tilde{\theta}}{2}} + |1\rangle e^{-i\frac{\tilde{\theta}}{2}} Z_4)_1 \\ &\quad\times(|0\rangle + |1\rangle Z_5)_4(|0\rangle + |1\rangle)_5 \\ &= |\varphi_\pm\rangle_3 X_1^{m_2} Z_1{}^{m_3} R_{\tilde{\theta},1}(|0\rangle + |1\rangle Z_4)_1 \\ &\quad\times(|0\rangle + |1\rangle Z_5)_4(|0\rangle + |1\rangle)_5. \end{aligned} \tag{7}$$

Next, measure qubit 4 on the X basis. The resulting state will be

$$\begin{aligned}&|\pm\rangle_4 X_1^{m_2} Z_1^{m_3} R_{\tilde{\theta},1} X_1^{m_4}(|00\rangle + |11\rangle)_{15}\\ &= |\pm\rangle_4 \left(X_1^{m_2} R_{\tilde{\theta},1} X_1^{m_2}\right) X_1^{m_2} Z_1^{m_3} X_1^{m_4}(|00\rangle + |11\rangle)_{15}\\ &= |\pm\rangle_4 R_{\theta,1} X_1^{m_2} Z_1^{m_3} X_1^{m_4}(|00\rangle + |11\rangle)_{15}. \end{aligned} \tag{8}$$

We rewrite the state of qubits 1 and 5 as

$$X_5^{m_4} Z_5^{m_3} X_5^{m_2} R_{\theta,5}(|00\rangle + |11\rangle)_{15}. \tag{9}$$

After correcting Pauli errors, $B_{\mathbf{m}} = X_5^{m_2} Z_5^{m_3} X_5^{m_4}$ on qubit 5, we get the resource state for Z rotation.

We define fidelity for a gate operation as

$$F_U = \mathrm{Tr}\, \rho_U |\Psi_U\rangle\langle\Psi_U|, \tag{10}$$

where $|\Psi_U\rangle$ is the perfect resource state, and ρ_U is the state we measure. From our example we know that

$$\rho_U = \mathrm{Tr}_p \sum_{\mathbf{m}} B_{\mathbf{m}} P_{\mathbf{m}} \rho P_{\mathbf{m}} B_{\mathbf{m}}^\dagger, \tag{11}$$

where $\mathbf{m}$ is the measuring outcome sequence, $P_{\mathbf{m}}$ is the projection operator, and $B_{\mathbf{m}}$ is the error-correction operator. Tr_p, the partial trace operation, traces out qubits other than the qubits in the resource state. Returning to our Z-rotation resource state, $P_{\mathbf{m}}$ stands for the measurement sequence on qubits 2, 3, and 4, and $B_{\mathbf{m}}$ stands for the correction operator $X_5^{m_2} Z_5^{m_3} X_5^{m_4}$. After the measurement and Pauli-error correction, a partial trace is taken so only qubits 1 and 5 exist in ρ_U.

If our qubit chain is in a perfect cluster state, we will have $\rho_U = |\Psi_U\rangle\langle\Psi_U|$, so our fidelity defined above turns out to be 1 in this case, coinciding with the perfect application of a Z-rotation operation. As the supplementary material in Ref. [19] points out, Jamiolkowski isomorphism ensures the correctness of the gate fidelity so defined.

Finally, it is enlightening to write the gate fidelity as

$$F_U = \mathrm{Tr}\left(\rho_U \frac{S_1 + I}{2} \frac{S_2 + I}{2}\right), \tag{12}$$

where S_1 and S_2 are stabilizers of $|\Psi_U\rangle$. Equation (12) can be further simplified for each type of gate (see Eqs. (18)–(21) in the supplementary material in Ref. [19]), which simplifies the calculation greatly.

III. CZ-GATE CREATION SCHEME

In 2001, Briegel and Raussendorf proposed the first scheme to create cluster states [22]. First, prepare all qubits in state $|+\rangle$. Then entangle them by applying the Ising Hamiltonian for a certain time interval, of which the accumulated effect is a CZ operation for each pair of neighboring sites. After these two steps, a cluster state is prepared. In fact, one can easily generalize this preparation: any method that applies CZ operations to all neighboring sites can fulfill this scheme.

A cluster state prepared in this way will deteriorate with time. We study the deterioration process in this section. We assume that the creation process produces a perfect cluster state. After the state is prepared, the system evolves over time and deteriorates because of coupling to a boson environment.

A. Pure phase noise: The exactly solvable case

We first limit the coupling term to pure phase noise. Without the presence of amplitude noise, we can solve the time-evolution problem exactly. We take amplitude noise into consideration in Sec. III C. The Hamiltonian here reads

$$H = \sum_{n=1}^{N} \epsilon_n \sigma_z^{(n)} + \sum_{\mathbf{k}} \omega_{\mathbf{k}} a_{\mathbf{k}}^\dagger a_{\mathbf{k}} + \sum_{n,\mathbf{k}} \sigma_z^{(n)} (g_{\mathbf{k}} a_{\mathbf{k}}^\dagger + g_{\mathbf{k}}^* a_{\mathbf{k}}), \tag{13}$$

where N is the qubit number, ϵ_n is half of the energy gap between the $|0\rangle$ and the $|1\rangle$ states of the nth qubit, and $\sigma_z^{(n)}$ is the Pauli Z operator of the nth qubit. $\omega_{\mathbf{k}}$ is the frequency or energy of a boson mode. We set $\hbar = 1$ in this paper. $a_{\mathbf{k}}^{(\dagger)}$ is the annihilation (creation) operator. The third term is the coupling term, with $g_{\mathbf{k}}$ being the coupling coefficient. This Hamiltonian is similar to the Dicke model [25], and the coupling term has been comprehensively studied in the single-qubit case [26]. Presumably, the coupling is weak in quantum computation situations, but our analysis applies to all coupling strengths.

Our qubits are initially prepared in a perfect cluster state:

$$\rho^Q(t=0) = |\Psi_C\rangle\langle\Psi_C|. \tag{14}$$

Our boson environment is initially set in a thermal state,

$$\begin{aligned}\rho^B(t=0) &= \frac{\exp\left(-\beta \sum_{\mathbf{k}} \epsilon_k a_{\mathbf{k}}^\dagger a_{\mathbf{k}}\right)}{\mathrm{Tr}\left[\exp\left(-\beta \sum_{\mathbf{k}} \epsilon_k a_{\mathbf{k}}^\dagger a_{\mathbf{k}}\right)\right]}\\ &= \prod_{\mathbf{k}} \frac{\exp(-\beta \epsilon_k a_{\mathbf{k}}^\dagger a_{\mathbf{k}})}{1 + \langle N_{\omega_k}\rangle}, \end{aligned} \tag{15}$$

where $\beta = 1/k_B T$, and $\langle N_{\omega_k}\rangle$ is the mean boson number with frequency ω_k in the thermal state.

We solve the time-evolution problem in the interaction picture. Choosing H_0 as

$$H_0 = \sum_{n=1}^{N} \epsilon_n \sigma_z^{(n)} + \sum_{\mathbf{k}} \epsilon_{\mathbf{k}} a_{\mathbf{k}}^\dagger a_{\mathbf{k}}, \tag{16}$$

we get the interaction part of the Hamiltonian,

$$\begin{aligned}V_I(t) &= e^{iH_0 t} \left(\sum_{n,\mathbf{k}} \sigma_z^{(n)} (g_{\mathbf{k}} a_{\mathbf{k}}^\dagger + g_{\mathbf{k}}^* a_{\mathbf{k}})\right) e^{-iH_0 t}\\ &= \sum_{n,\mathbf{k}} \sigma_z^{(n)} (g_{\mathbf{k}} e^{i\omega_k t} a_{\mathbf{k}}^\dagger + g_{\mathbf{k}}^* e^{-i\omega_k t} a_{\mathbf{k}}). \end{aligned} \tag{17}$$

The unitary time-evolution operator is

$$\begin{aligned}U_I(t) &= \hat{T} \exp\left[-i \int_0^t V_I(t')dt'\right]\\ &= \exp\left\{\sum_{n,\mathbf{k}} \left[g_{\mathbf{k}} \sigma_z^{(n)} \varphi_{\omega_k}(t) a_{\mathbf{k}}^\dagger - g_{\mathbf{k}}^* \sigma_z^{(n)} \varphi_{\omega_k}^*(t) a_{\mathbf{k}}\right]\right\}\\ &\quad \times \exp\left\{i \sum_{\mathbf{k}} \sum_{m,n} |g_{\mathbf{k}}|^2 \sigma_z^{(m)} \sigma_z^{(n)} s(\omega_k, t)\right\}, \end{aligned} \tag{18}$$

where

$$\varphi_{\omega_k}(t) = \frac{1 - e^{i\omega_k t}}{\omega_k}, \tag{19}$$

$$s(\omega_k, t) = \frac{\omega_k t - \sin(\omega_k t)}{{\omega_k}^2}. \tag{20}$$

We present the detailed derivation of this part in the Appendix (Sec. 1). The reduced density matrix of the qubit part evolves as

$$\rho_I^Q(t) = \mathrm{Tr}_E\big[U_I(t)\rho_I^Q(0) \otimes \rho_I^E(0){U_I}^\dagger(t)\big]. \tag{21}$$

After some calculation, we get the component form of the density operator,

$$\begin{aligned}\rho^Q_{I,\{i_n,j_n\}}(t) &\equiv \langle i_1, i_2, \ldots, i_N|\rho_I^Q(t)|j_1, j_2, \ldots, j_n\rangle \\ &= \exp\left\{-\Gamma(t,T)\left[\sum_{n=1}^{N}(i_n - j_n)\right]^2\right\} \\ &\times \exp\left\{i\Theta(t)\left[\left(\sum_{n=1}^{N} i_n\right)^2 - \left(\sum_{n=1}^{N} j_n\right)^2\right]\right\} \\ &\times \rho^Q_{I,\{i_n,j_n\}}(0).\end{aligned} \tag{22}$$

The subscript I indicates the interaction picture. The expression of $\Gamma(t,T)$ and $\Theta(t)$ and the detailed calculation of Eq. (21) are presented in the Appendix (Sec. 2). We proceed to take the continuum limit in the Appendix, after which $g_{\mathbf{k}}$ is contained in the spectral density. Afterwards, we assume an ohmic spectral density here:

$$I(\omega) = \eta\omega e^{-\omega/\omega_c}. \tag{23}$$

After some calculation, we reach

$$\Gamma(t,T) = \eta \ln\left(1 + {\omega_c}^2 t^2\right) + \eta \ln\left(\frac{\beta}{\pi t}\sinh\frac{\pi t}{\beta}\right), \tag{24}$$

$$\Theta(t) = \eta\omega_c t - \eta \arctan(\omega_c t). \tag{25}$$

The fidelity of a cluster state here is defined as

$$F = \mathrm{Tr}(|\Psi_C\rangle\langle\Psi_C|\rho^Q(t)). \tag{26}$$

Here ρ^Q is the reduced density operator of the qubits. Remember that if the perfect cluster state is in the Schrödinger picture, we of course require ρ_Q to be presented in the Schrödinger picture. Rewriting the equation using the density operator in the interaction picture, we have

$$F(t) = \mathrm{Tr}\big(|\Psi_C\rangle\langle\Psi_C|e^{-iH_0 t}\rho_I^Q(t)e^{iH_0 t}\big). \tag{27}$$

We plot a seven-qubit linear cluster state coupled with a boson environment (Fig. 3). The parameters are $\eta = 1/1000$, $\omega_c = 100$, and $\beta/\pi = 1$. There are three lines in the figure: $\epsilon_n = 3$ [solid (green)], $\epsilon_n = 0.9$ [dashed (blue)], and $\epsilon_n = 0$ [dash-dotted (red)].

Two factors contribute to the oscillation of fidelity over time: the Θ function and the H_0 part. If the two oscillation frequencies are close, the oscillation pattern is highly unpredictable [see the dashed (blue) lines]. For any real systems, this case should be avoided. We emphasize that when coupling does not exist, the fidelity still oscillates due to the H_0 part, but the peak of the oscillation is always 1. Another fact is that even when the temperature of the boson environment is 0, there is still a fidelity drop at the peak. This is easy to understand, since the coupling term still works for the system, even though all modes of the boson environment are in the vacuum state.

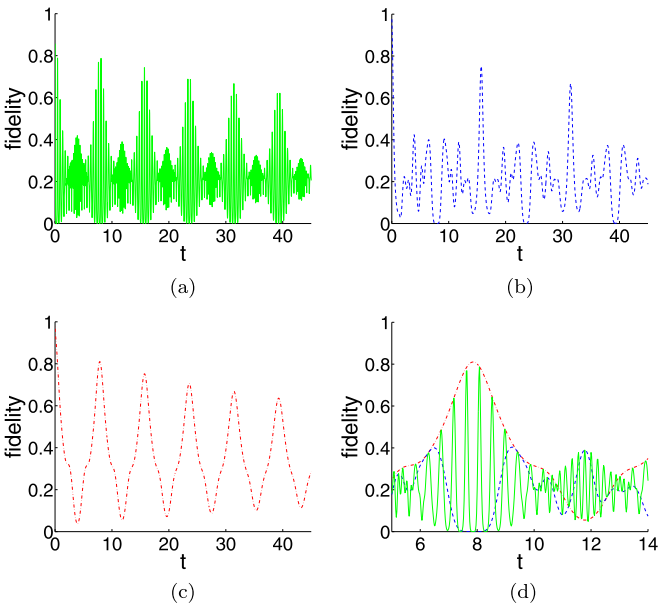

FIG. 3. (Color online) Fidelity-time relation of a seven-qubit linear cluster state. Solid (green) lines, $\epsilon_n = 3$; dashed (blue) lines, $\epsilon_n = 0.9$; and dash-dotted (red) lines, $\epsilon_n = 0$. (a) $\epsilon_n = 3$. (b) $\epsilon_n = 0.9$. (c) $\epsilon_n = 0$. (d) Zoom-in on the whole figure, with the three ϵ_n values presented.

To be more specific, we analyze the fidelity for various gate operations:

$$F_U = \mathrm{Tr}(\rho_U(t)|\Psi_U\rangle\langle\Psi_U|). \tag{28}$$

The fidelity-time dependence for a five-qubit identity gate, an eight-qubit Hadamard gate, a Z-rotation gate, and a CZ gate are plotted in Fig. 4. The parameters are $\eta = 1/1000$, $\omega_c = 100$, and $\beta/\pi = 1$. Because a medium ϵ_n will result in an unpredictable time-evolution pattern, this kind of fidelity curve is not presented. Different gate operations show different oscillation patterns, due to their own lattice structures and sizes.

Figure 4 shows that when ϵ_n is large, all types of gates exhibit a fidelity peak uniformly at $t \approx 8$, which is better than the $\epsilon_n = 0$ case. This is because when ϵ_n is large, the H_0 causes the fidelity to oscillate rapidly, which leaves the gate-type-independent Θ function to shape the envelope of the fidelity. Therefore, if the measurement can be implemented rapidly, a strong ϵ_n is preferred.

B. Suggestions for enhancing the performance of the CZ-gate creation scheme

Because of the advantage listed above, we chose the solid (green) line in Fig. 4 to conduct our investigation here. In this section, we focus on making suggestions for enhancing the performance of MBQCs realized by the CZ-gate creation scheme.

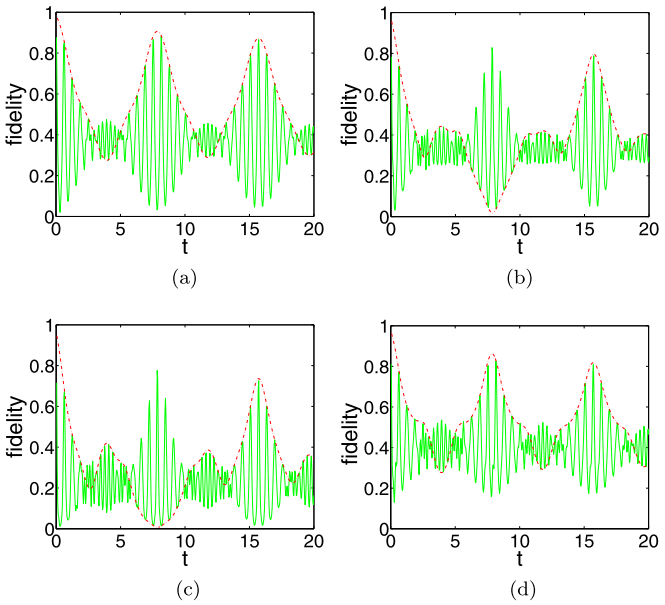

FIG. 4. (Color online) Fidelity-time dependence. Solid (green) lines, $\epsilon_n = 5$; dash-dotted (red) lines, $\epsilon_n = 0$. (a) Five-qubit identity gate. (b) Eight-qubit Hadamard gate. (c) CZ gate. (d) Z-rotation gate, $\zeta = \pi/8$.

If the gate operation is implemented as soon as the cluster state is prepared, one would be concerned about the drop rate of the fidelity in the first several fidelity peaks. We treat the fidelity drop rate as

$$\left.\frac{\Delta F}{\Delta t}\right|_{t\to 0} = \frac{F(t=t_1) - F(t=0)}{t_1}, \tag{29}$$

where t_1 is the time to the first peak of fidelity after $t = 0$. We calculate the fidelity drop rate versus the temperature of the boson environment. Our result is shown in Fig. 5. As the figure reveals, the fidelity drop rate curves decrease as the temperature increases, but the decrease is slow and nonlinear. When the environmental temperature gets lower, the decrease becomes even slower. This process eventually stops at $T = 0$, where the fidelity drop rates reach a nonzero value. Utilizing this fact, we can save cooling equipment, since

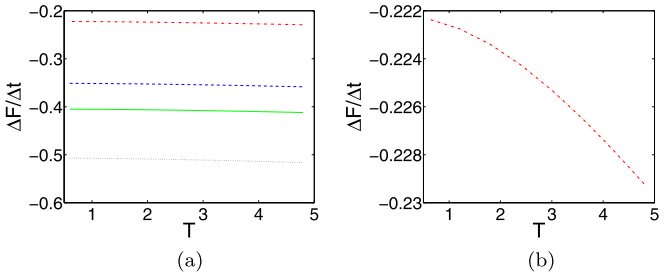

FIG. 5. (Color online) The derivative of fidelity as a function of temperature. Dash-dotted (red) lines, five-qubit identity gate; solid (green) lines, eight-qubit Hadamard gate; dashed (blue) lines, Z-rotation gate; and dotted black lines, CZ gate. (a) The derivative of four gate operations. (b) Extraction: the derivative of the five-qubit identity gate only.

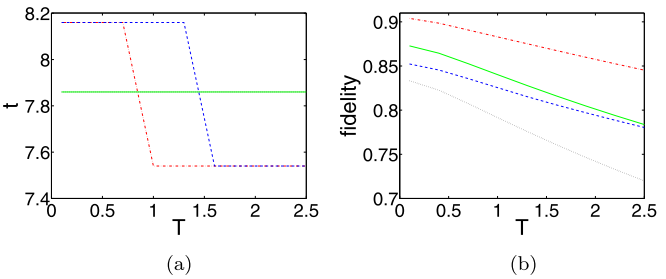

FIG. 6. (Color online) Peak statistics. Dash-dotted (red) lines, five-qubit identity gate; solid (green) lines, eight-qubit Hadamard gate; dashed (blue) lines, Z-rotation gate; and dotted black lines, CZ gate. (a) Arrival time of the peak dependent on the temperature, with the solid (green) line and the dotted black line overlapping. (b) Peak fidelity dependent on the temperature.

there is little room for the fidelity drop rates to decrease at low temperature.

If a cluster state could be kept for some time before measuring it, we would ask where the fidelity peaks become high enough. This question fits the situation when a part of the computation must wait until other parts are finished, and the cluster state is already prepared. From Fig. 4 we learn that the fidelity peaks in the first peak of the envelope (see the set of fidelity peaks near $t \approx 8$) may be suitable for our purpose. To evaluate this area, we calculate the arrival time of the highest peak in it and the fidelity of the highest peak.

Our calculation (see Fig. 6) proves the suitability of this area in two respects. First, the fidelity of the highest peak is high enough. From Fig. 6, we see that the fidelities are all above 0.8 when $T < 0.5$. We also work out the fidelity-temperature dependence at very low temperatures (see Fig. 7). When the temperature goes even lower, the fidelity no longer changes, stopping at a value lower than 1 at $T = 0$. Therefore, again, we need not cool down the temperature with great effort. In our parameter setting, $\omega_T = 0.1$ is good enough to ensure a high fidelity for the highest peak.

Second, the arrival time of the highest peak is almost independent of the environmental temperature and completely independent of the gate type, which simplifies its utilization. The highest peak may switch from one to another among several neighboring peaks, as happens for the identity gate and the Z-rotation gate in Fig. 7, but this fact does not complicate

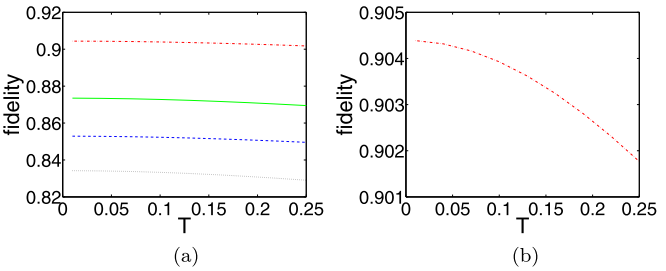

FIG. 7. (Color online) Fidelity-temperature dependence. Dash-dotted (red) lines, five-qubit identity gate; solid (green) lines, eight-qubit Hadamard gate; dashed (blue) lines, Z-rotation gate; and dotted black lines, CZ gate. (a) Four types of gates. (b) Extraction: five-qubit identity gate only.

our procedure. Since several peaks near the highest peak are almost equally good and the temperature should not vary much, we can just stick with one of the peaks. The fact that the highest peak arrives uniformly regardless of T is because the oscillation is mainly controlled by the Θ function and H_0, both of which do not depend on the environmental temperature at all. The arrival time is also independent of gate type. Again, it is because of the Θ function, which remains invariant under changes in gate type, qubit number, and lattice shape of the cluster state.

C. Generalized noise: Numerical results

Until now, we have only evaluated pure phase noise. From the perspective of noise theory, pure phase noise fails to describe all circumstances. As a result, we generalize our Hamiltonian to consider both phase and amplitude noise in this section:

$$H = \sum_{n=1}^{N} \epsilon_n \sigma_z^{(n)} + \sum_{\mathbf{k}} \omega_k a_{\mathbf{k}}^\dagger a_{\mathbf{k}} + \sum_{n,\mathbf{k}} \left(\cos(\theta)\sigma_z^{(n)} - \sin(\theta)\sigma_x^{(n)}\right)(g_{\mathbf{k}} a_{\mathbf{k}}^\dagger + g_{\mathbf{k}}^* a_{\mathbf{k}}). \quad (30)$$

With amplitude noise added, we can no longer solve the time-evolution problem analytically. Instead, we seek numerical solutions, trying to figure out the character of the generalized noise. For simplicity, we calculate a single-mode boson environment, with the frequency resonant with the energy gap of a two-level qubit:

$$H = \epsilon \sum_{n=1}^{N} \sigma_z^{(n)} + 2\epsilon a^\dagger a + g(a^\dagger + a) \sum_{n} \left(\cos(\theta)\sigma_z^{(n)} - \sin(\theta)\sigma_x^{(n)}\right). \quad (31)$$

This single-frequency model is reasonable, because naturally the resonant frequency mode causes more damage. The only drawback of this model is that it fails to describe the situation when $\epsilon = 0$, in which case a boson would have zero energy, which is impossible.

For cluster states consisting of several qubits, we write a program to calculate the time evolution of the density operator:

$$\rho^Q(t) = e^{-iHt}\rho^Q(0)e^{iHt}. \quad (32)$$

In the system, the boson environment is infinite-dimensional. In our program, however, we adopt a cutoff approximation, setting the maximum boson number to some large number.

The gate fidelity is still defined by Eq. (10). We show the calculation outcomes for the five-qubit identity gate, eight-qubit Hadamard gate, Z-rotation gate, and CZ gate. We set $g = 0.1$, $\epsilon = 5$, and $T = 1$, with different θ's considered (see Fig. 8).

The fidelity curves in Fig. 8 show some common patterns. First, all angles θ result in similar oscillation patterns, with the same oscillation frequency. The reason is transparent. Since the coupling is weak, we are safe to assume that the oscillation frequency is mainly governed by the H_0 part of the Hamiltonian, which remains independent of the noise type (or, equivalently, the parameter θ).

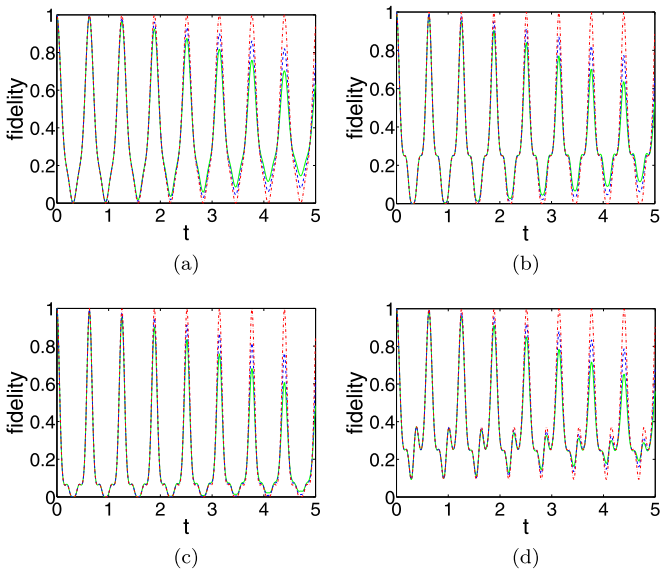

FIG. 8. (Color online) Fidelity-time dependence. Solid (green) lines, $\theta = \pi/2$; dashed (blue) lines, $\theta = \pi/4$; and dash-dotted (red) lines, $\theta = 0$. (a) Five-qubit identity gate. (b) Eight-qubit Hadamard gate. (c) CZ gate. (d) Z-rotation gate, $\zeta = \pi/8$.

An interesting fact is that phase noise imposes less damage than amplitude noise. According to Fig. 8, the case where $\theta = 0$ has its peak fidelity near 1 even after a long time. This character can be understood through some qualitative reasoning. Since a Z error cannot change the energy of the qubits, while the boson environment must add or subtract its boson number by 1 to impose an error, the total energy of the system is changed by 2ϵ. In contrast, an X error changes the energy of the qubits by 2ϵ, which compensates for the energy change in the boson environment and maintains the energy of the whole system unchanged. Since X errors do not require the energy of the system to change, they occur much more easily than Z errors.

IV. CLUSTER HAMILTONIAN CREATION SCHEME

A cluster state can also be created by cluster Hamiltonians [2,7], of which the cluster state is the ground state. The simplest cluster Hamiltonian is

$$H_{fC} = -J \sum_i K_i, \quad (33)$$

where $J > 0$, and K_i are the stabilizers of the cluster state:

$$K_i = X_i \prod_{\text{neigh}} Z_j. \quad (34)$$

The product is over all sites neighboring site i. Since the ground state $|g\rangle$ must be a state where

$$K_i|g\rangle = |g\rangle, \quad \forall i, \quad (35)$$

we claim that $|g\rangle = |\Psi_C\rangle$. Therefore, upon cooling this system, we obtain a thermal state close to a cluster state.

To construct an appropriate model for noise, we need to study the energy level of Hamiltonian (33). The eigenstate of H_{fC} is just the common eigenstates of all cluster stabilizers

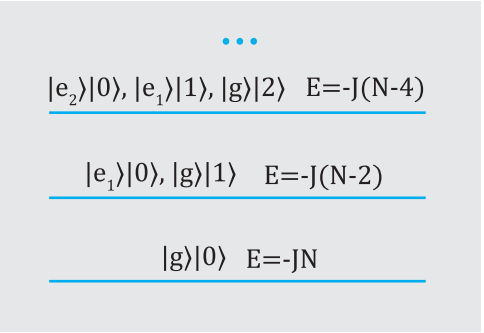

FIG. 9. (Color online) Energy levels of H_C, with $g = 0$.

$\{K_i\}$. The first excited state, $|e_1\rangle$, will be the eigenstate with eigenvalue -1 of a certain K_i and the eigenvector with eigenvalue 1 of $K_j, \forall j \neq i$. Its energy is $2J$ higher than the ground state. Following this reasoning, we conclude that the energy gaps between neighboring energy levels are all $2J$. Degeneracy of this model can also be deduced. For example, since $|e_1\rangle$ can only have one eigenvalue -1, and there are n stabilizers for a certain cluster state, we conclude that the first excited state is N-fold degenerate. Applying the same method, one can calculate the degeneracy of higher excited states. We remark that the ground state is nondegenerate.

Now we can construct a single-mode boson environment, with the mode frequency resonant with the gap between the nearest energy levels:

$$H_C = -J \sum_i K_i + 2Ja^\dagger a + g(a^\dagger + a) \times \sum_n \left(\cos(\theta)\sigma_z^{(n)} - \sin(\theta)\sigma_x^{(n)}\right). \quad (36)$$

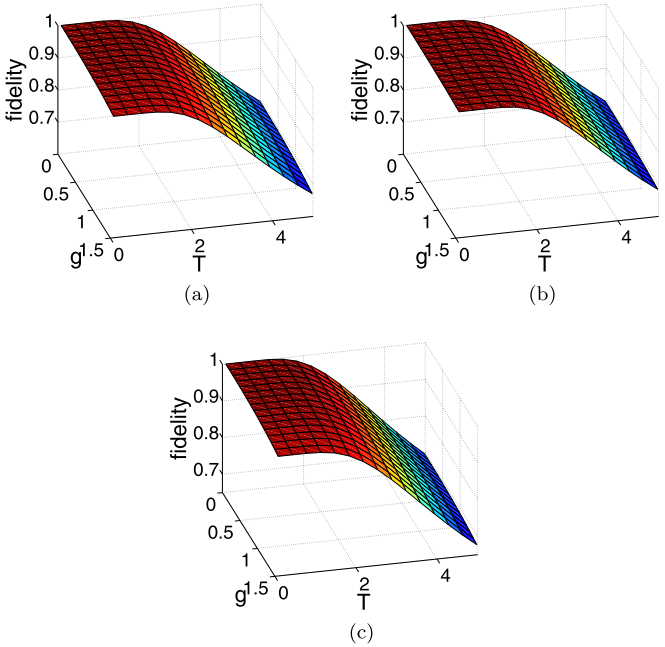

FIG. 10. (Color online) Fidelity of a five-qubit identity gate, dependent on T and g. (a) $\theta = \pi/2$. (b) $\theta = \pi/4$. (c) $\theta = 0$.

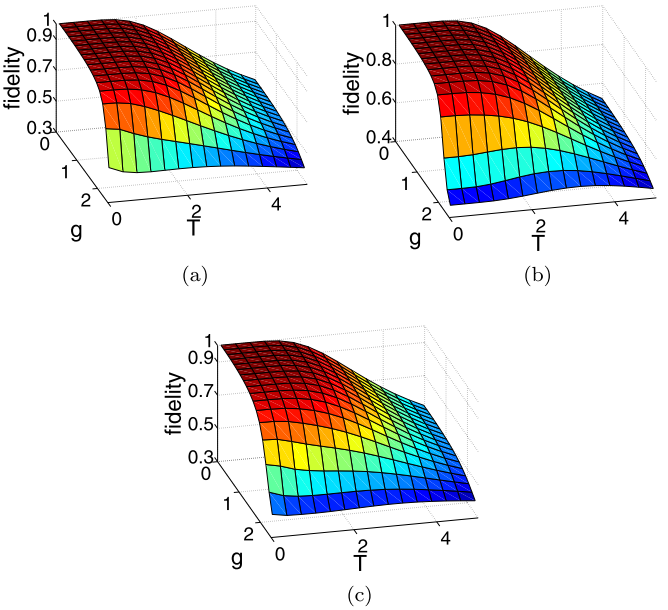

FIG. 11. (Color online) Fidelity of an eight-qubit Hadamard gate, dependentg on T and g. (a) $\theta = \pi/2$. (b) $\theta = \pi/4$. (c) $\theta = 0$.

The energy level structure of this Hamiltonian, with $g = 0$, is plotted in Fig. 9. In the figure, $|0\rangle$, $|1\rangle$, and $|2\rangle$ are the boson number states in Fock space. The ground state is a cluster state, $|g\rangle = |\Psi_C\rangle$, coupled with a vacuum $|0\rangle$, and the first excited state is either $|e_1\rangle$ with a vacuum or $|g\rangle$ with one boson. The gap between the nearest energy levels is also $2J$.

The density operator for the thermal state is

$$\rho_{\text{th}} = e^{-\beta H_C} / \text{Tr}(e^{-\beta H_C}). \quad (37)$$

Again, we compute the fidelity for gate operations of this density operator. At low temperatures, the thermal state mainly comprises the lowest several energy levels. As a result, we again use a cutoff on the boson number in our computation.

In Figs. 10 and 11, we plot the fidelity of a five-qubit identity gate and an eight-qubit Hadamard gate as a function of the temperature T and coupling coefficient g. For clarity, we also present the fidelity-g dependence for different T's in Fig. 12, setting $\theta = \pi/2$.

We find that the Hamiltonian creation scheme produces cluster states robust against the boson environment, when the

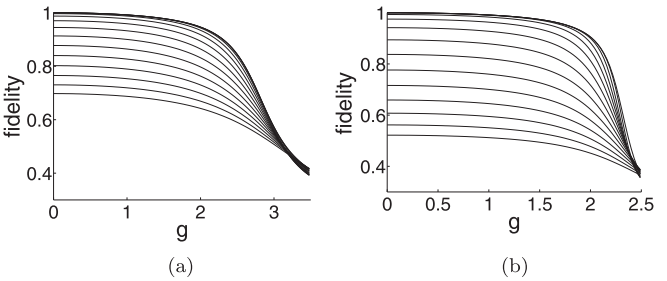

FIG. 12. Fidelity-g dependence. Different lines vary only in temperature. $\theta = \pi/2$. (a) Five-qubit identity gate. (b) Eight-qubit Hadamard gate. For small g, the fidelity drop is negligible.

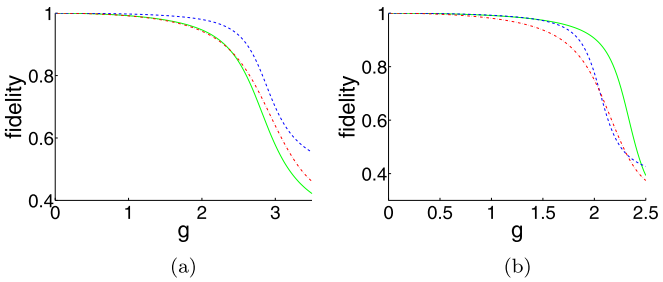

FIG. 13. (Color online) Fidelity-g dependence for different θ. Solid (green) lines, $\theta = \pi/2$; dashed (blue) lines, $\theta = \pi/4$; and dash-dotted (red) lines, $\theta = 0$. (a) Five-qubit identity gate. (b) Eight-qubit Hadamard gate.

coupling is below a certain threshold amount, whether it is under phase or amplitude noise. The fidelity is close to 1 as long as g and T are below a critical coupling coefficient value, depending on the gate type (see Fig. 13). Further, a small g value does not deteriorate the fidelity even when the temperature T is high. This is shown in Fig. 12, where, with small g, the curves overlap greatly.

When the coupling becomes gradually stronger, a sudden drop in fidelity is observed. This character is similar to the sudden change in fidelity when T goes high, which is well treated in Ref. [19]. Figures 12 and 13 show that for a five-qubit identity gate, $g_c \approx 2.9$, while for an eight-qubit Hadamard gate, $g_c \approx 2.4$. Below these critical coupling coefficients, the fidelity does not suffer from the coupling effect. For example, setting $\theta = \pi/4$ and $\epsilon = 5$, the fidelity of a five-qubit identity gate at $g = 0$, $T = 1.83$ is 0.9874, while at $g = 2.4$, $T = 1.83$ it is 0.9203, which means the fidelity only drops by 0.0671 with superstrong coupling. Actually, $g/J \sim 1$, known as ultrastrong coupling, and requiring special design to be achieved in experiments [27], would not occur in a quantum computation task. As a result, the sudden drop in fidelity does not harm the gate operations evaluated here. However, in a large cluster state, this character may become an issue. Since g_c depends on the cluster size, it is probable that a large cluster state has a small critical value. In this case, one must calculate the critical coefficient carefully and restrict the coupling effect to below this level in the MBQC system.

V. DISCUSSION

In this section we first analyze the difference between gate fidelity and cluster-state fidelity. We then discuss the collective character of our environment.

One may wonder why the gate fidelity is different from the corresponding cluster-state fidelity, as their definitions are similar. The first observation to answer this question is that, to get a correct gate teleportation resource state by the procedure shown in Fig. 2, one does not necessarily need a cluster state. Again, we take the Z-rotation gate as an example. If there are X errors on both qubit 2 and qubit 4, the resource state can also be correctly prepared:

$$\begin{aligned}\rho_U &= \mathrm{Tr}_p \sum_{\mathbf{m}} B_{\mathbf{m}} P_{\mathbf{m}} (X_2 \otimes X_4) |\Psi_C\rangle\langle\Psi_C| (X_2 \otimes X_4) P_{\mathbf{m}} B_{\mathbf{m}}^\dagger \\ &= \mathrm{Tr}_p \sum_{\mathbf{m}} (X_2 \otimes X_4) B_{\mathbf{m}} P_{\mathbf{m}} |\Psi_C\rangle\langle\Psi_C| P_{\mathbf{m}} B_{\mathbf{m}}^\dagger (X_2 \otimes X_4) \\ &= \mathrm{Tr}_p \sum_{\mathbf{m}} B_{\mathbf{m}} P_{\mathbf{m}} |\Psi_C\rangle\langle\Psi_C| P_{\mathbf{m}} B_{\mathbf{m}}^\dagger, \end{aligned} \tag{38}$$

where the relationship $P_{\mathbf{m}}(X_2 \otimes X_4) = (X_2 \otimes X_4) P_{\mathbf{m}}$ holds, since the measurement of qubits 2 and 4 is under the X basis. In this section, we denote the Pauli X operator as X and the Z operator as Z. The same reasoning holds when the error is $Z_2 \otimes Z_4$. It is thus natural that the gate fidelity does not equal to the corresponding cluster-state fidelity.

Further, we quantify the difference by the eigenstates of the cluster state's stabilizers, since they form a complete orthonormal basis. We denote the eigenstates

$$|\psi_i\rangle, \quad \forall i \in \{1,2,\ldots,2^n\}, \tag{39}$$

with n being the qubit number. We denote the cluster state in it $|\psi_1\rangle$, satisfying

$$K_j |\psi_1\rangle = 1, \quad \forall j \in \{1,2,\ldots,n\}. \tag{40}$$

We decompose an arbitrary density matrix as

$$\rho = \sum_{i,j} a_{ij} |\psi_i\rangle\langle\psi_j|. \tag{41}$$

For the cluster-state fidelity,

$$F = \mathrm{Tr}(|\Psi_C\rangle\langle\Psi_C|\rho) = \mathrm{Tr}(|\psi_1\rangle\langle\psi_1|\rho) = a_{11}. \tag{42}$$

For the gate fidelity, in contrast,

$$\begin{aligned} F_U &= \mathrm{Tr}(|\Psi_U\rangle\langle\Psi_U|\rho_U) = \mathrm{Tr}\left(|\Psi_U\rangle\langle\Psi_U| \,\mathrm{Tr}_p \sum_{\mathbf{m}} B_{\mathbf{m}} P_{\mathbf{m}} \rho P_{\mathbf{m}} B_{\mathbf{m}}^\dagger\right) \\ &= \mathrm{Tr}\left(|\Psi_U\rangle\langle\Psi_U| \,\mathrm{Tr}_p \sum_{\mathbf{m}} B_{\mathbf{m}} P_{\mathbf{m}} a_{11} |\psi_1\rangle\langle\psi_1| P_{\mathbf{m}} B_{\mathbf{m}}^\dagger\right) + \mathrm{Tr}\left(|\Psi_U\rangle\langle\Psi_U| \,\mathrm{Tr}_p \sum_{\mathbf{m}} B_{\mathbf{m}} P_{\mathbf{m}} {\sum_{i,j}}' a_{ij} |\psi_i\rangle\langle\psi_j| P_{\mathbf{m}} B_{\mathbf{m}}^\dagger\right), \end{aligned} \tag{43}$$

where the primed sum does not go over $i = j = 1$. By the process of gate teleportation, the first part on the right-hand side equals a_{11}. The second part, which is nonzero generally, results in the difference between the gate fidelity and the corresponding cluster-state fidelity.

We plot four fidelity-temperature curves to give a direct demonstration; see Fig. 14. The gate fidelities here all go above

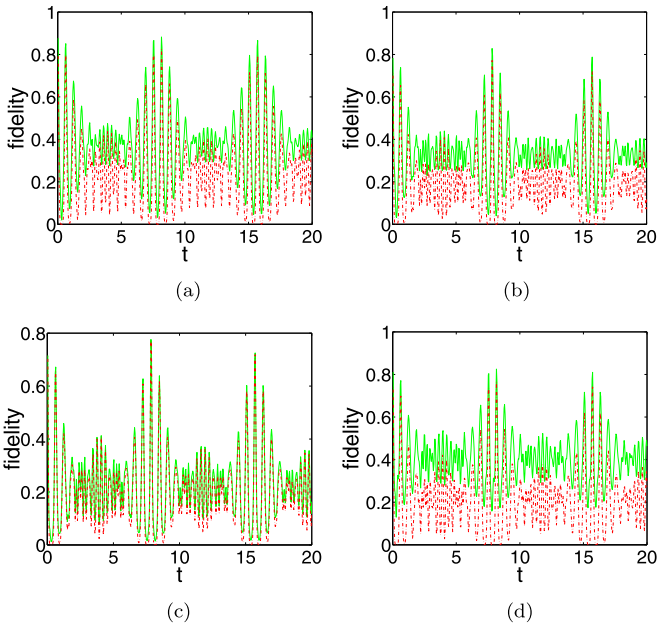

FIG. 14. (Color online) Comparison between the gate fidelity [solid (green) lines] and the corresponding cluster fidelity [dash-dotted (red) line], with $\epsilon_n = 5$. (a) Five-qubit identity gate. (b) Eight-qubit Hadamard gate. (c) CZ gate. (d) Z-rotation gate, $\theta = \pi/8$.

the corresponding cluster-state fidelities, but generally they show the same pattern.

Now we analyze the collective character of our noise models. Our Hamiltonians, such as Eq. (30), do not distinguish qubits from each other and, thus, remain invariant when the qubits are permuted. In Ref. [28], this is called the "collective decoherence" case, to distinguish it from the individual decoherence case. The collective character of our Hamiltonian may result in an outcome that is different from the individual case. As evidence, we evaluate the fidelity drop versus the qubit number in a linear cluster state. We use Hamiltonian (30). We set $\theta = \pi/2$, $g = 0.1$, $\epsilon = 5$, and the temperature of the boson environment $T = 1$. The typical fidelity oscillation pattern is like Fig. 15. Again, the fidelity peaks occur at a certain time, indifferent to a change in the qubit number.

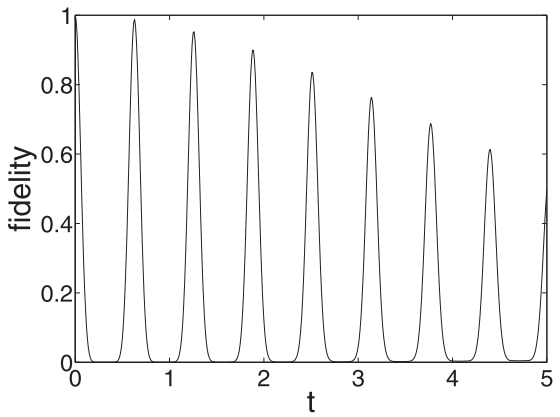

FIG. 15. A typical oscillation pattern in this setting, showing the fidelity-time relationship for a six-qubit linear cluster state.

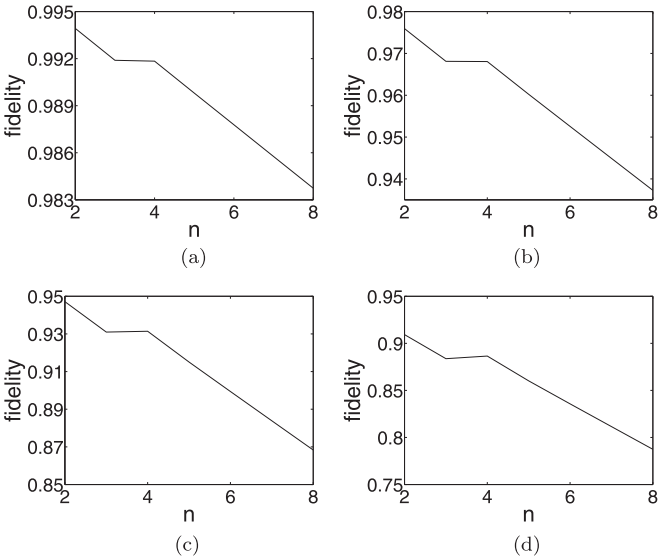

FIG. 16. Cluster fidelity for the first four peaks versus qubit number n. The fidelity drop turns out to be linear.

As expected in the independent case, the fidelity drops exponentially with an increase in qubits. However, here, the fidelity only drops linearly with the increase in qubit number (Fig. 16). This fact may just be due to the character of our "collective" noise model.

VI. CONCLUSION

In this paper, we analyze the fidelity of the MBQC scheme when the system is coupled with a boson environment. Two specific schemes, the CZ creation scheme and the Hamiltonian creation scheme, are studied.

In the CZ creation scheme, we solve the time evolution of the fidelity. We provide the exact solution for the pure phase noise case and calculate numerically for the generalized noise case. We study four kinds of gate fidelity in detail and propose two suggestions to enhance the performance under coupling.

In the Hamiltonian creation scheme, the phenomenon of a sudden change in fidelity is discovered. Below a certain threshold coupling coefficient value, the damage caused by the boson environment is negligible. The threshold value depends on the gate type and cluster size. For individual gates consisting of several qubits, the threshold value is large so one will not worry about the effect caused by coupling. We conclude that the Hamiltonian creation method is robust against this kind of noise under a threshold coupling value.

MBQC is a promising quantum computation scheme, and the findings in this paper may be significant for the practical implementation of MBQC systems.

ACKNOWLEDGMENTS

This research was supported by the "973" program (2010CB922904), the NSFC, grants from the CAS and NFFTBS (Nos. J1030310 and J1103205), and the National Undergraduate Innovational Experimentation Program.

APPENDIX A: DERIVATIONS OF TWO FORMULAS

For completeness, we next present the detailed calculations for two formulas in the text. The calculations here are similar to those in Refs. [28] and [29]. One may also refer to Ref. [30] for some parts of the calculations. This part is self-consistent and is presented in the same style as in the text.

1. Derivation of the unitary evolution operator

The fact that $U_I(t)$ can be solved exactly is due to the pure dephasing character of the Hamiltonian interaction part. In this section, we prove formula (18). Substituting Eq. (17) into U_I, we get

$$U_I(t) = \hat{T}\exp\left[-i\int_0^t \sum_{n,\mathbf{k}} \sigma_z^{(n)}(g_{\mathbf{k}} e^{i\omega_k t'} a_{\mathbf{k}}^\dagger + g_{\mathbf{k}}^* e^{-i\omega_k t'} a_{\mathbf{k}})dt'\right]. \tag{A1}$$

In order to simplify the expression, we here prove the useful formula

$$\hat{T}\exp\left[\int_0^t dt_1(\hat{A}(t_1)+\hat{B}(t_1))\right] = \exp\left[\int_0^t \hat{A}(t_1)dt_1\right]\hat{T}\exp\left\{\int_0^t\left[\exp\left(-\int_0^{t_1}\hat{A}(t_2)dt_2\right)\hat{B}(t_1)\exp\left(\int_0^{t_1}\hat{A}(t_2)dt_2\right)\right]dt_1\right\}. \tag{A2}$$

First, we denote $\hat{X}(t) = \hat{T}\exp[\int_0^t \hat{A}(t_1)+\hat{B}(t_1)dt_1], \hat{Y}(t) = \exp[\int_0^t \hat{A}(t_1)dt_1]$, and $\hat{Z}(t) = \hat{Y}^{-1}(t)\hat{X}(t)$. We have

$$d\hat{X}/dt = [\hat{A}(t)+\hat{B}(t)]\hat{X}(t), \tag{A3}$$

$$d\hat{Y}dt = \hat{A}(t)\hat{Y}(t). \tag{A4}$$

As a result,

$$d\hat{Z}/dt = -\hat{A}(t)\hat{Y}^{-1}(t)\hat{X}(t) + \hat{Y}^{-1}(t)(\hat{A}(t)+\hat{B}(t))\hat{X}(t) = \hat{Y}^{-1}(t)\hat{B}(t)\hat{X}(t) = [\hat{Y}^{-1}(t)\hat{B}(t)\hat{Y}(t)]\hat{Z}(t). \tag{A5}$$

Integrating this equation, we have

$$\hat{Z}(t) = 1 + \int_0^t [\hat{Y}^{-1}(t_1)\hat{B}(t_1)\hat{Y}(t_1)]\hat{Z}(t_1)dt_1. \tag{A6}$$

Iterating this equation repeatedly, we get

$$\hat{Z}(t) = 1 + \int_0^t dt_1\hat{V}(t_1) + \int_0^t dt_1\int_0^{t_1} dt_2\hat{V}(t_1)\hat{V}(t_2) + \cdots = \hat{T}\exp\left[\int_0^t \hat{V}(t_1)dt_1\right], \tag{A7}$$

where $\hat{V}(t) = \hat{Y}^{-1}(t)\hat{B}(t)\hat{Y}(t)$. We can rewrite this equation as

$$\hat{X}(t) = \hat{Y}(t)\exp\left[\int_0^t \hat{Y}^{-1}(t)\hat{B}(t)\hat{Y}(t)dt_1\right]. \tag{A8}$$

Substituting the expressions of $\hat{X}(t)$ and $\hat{Y}(t)$ into it, we prove formula (A2).

Now we evaluate $U_I(t)$ in Eq. (A1). Setting

$$\hat{A}(t) = -i\sum_{n,\mathbf{k}} \sigma_z^{(n)} g_{\mathbf{k}} e^{i\omega_k t} a_{\mathbf{k}}^\dagger, \tag{A9}$$

$$\hat{B}(t) = -i\sum_{n,\mathbf{k}} \sigma_z^{(n)} g_{\mathbf{k}}^* e^{-i\omega_k t} a_{\mathbf{k}}, \tag{A10}$$

(A2) becomes

$$\begin{aligned} U_I(t) &= \hat{T}\exp\left[\int_0^t dt_1(\hat{A}(t_1)+\hat{B}(t_1))\right] \\ &= \exp\left[\int_0^t \hat{A}(t_1)dt_1\right]\hat{T}\exp\left\{\int_0^t\left[\exp\left(-\int_0^{t_1}\hat{A}(t_2)dt_2\right)\hat{B}(t_1)\exp\left(\int_0^{t_1}\hat{A}(t_2)dt_2\right)\right]dt_1\right\}. \end{aligned} \tag{A11}$$

Applying the Baker-Hausdorff formula $e^{\hat{A}}\hat{B}e^{-\hat{A}} = \hat{B} + [\hat{A},\hat{B}] + [\hat{A},[\hat{A},\hat{B}]]/2! + \ldots$ and noting that $[\hat{A},[\hat{A},\hat{B}]] = 0$, we conclude that

$$\exp\left(-\int_0^{t_1}\hat{A}(t_2)dt_2\right)\hat{B}(t_1)\exp\left(\int_0^{t_1}\hat{A}(t_2)dt_2\right) = B(t_1) - \sum_{n,m,\mathbf{k}} \frac{|g_{\mathbf{k}}|^2(1-e^{-i\omega_k t_1})}{i\omega_k}\sigma_z^{(n)}\sigma_z^{(m)}. \tag{A12}$$

As a result, time ordering is no longer required in the third line of Eq. (A11), and we rewrite it as

$$\begin{aligned} U_I(t) &= \exp\left[\int_0^t \hat{A}(t_1)dt_1\right]\exp\left\{\int_0^t\left[B(t_1)-\sum_{n,\mathbf{k}}\frac{|g_\mathbf{k}|^2(1-e^{-i\omega_k t_1})}{i\omega_k}\sigma_z^{(n)}\sigma_z^{(m)}\right]dt_1\right\} \\ &= \exp\left[\int_0^t \hat{A}(t_1)dt_1\right]\exp\left[\int_0^t B(t_1)dt_1-\sum_{n,m,\mathbf{k}}\frac{|g_\mathbf{k}|^2\left(t-\frac{e^{-i\omega_k t}-1}{-i\omega_k}\right)}{i\omega_k}\sigma_z^{(n)}\sigma_z^{(m)}\right] \\ &= \exp\left[\int_0^t \hat{A}(t_1)dt_1\right]\exp\left[\int_0^t B(t_1)dt_1\right]\exp\left[-\sum_{n,m,\mathbf{k}}\frac{|g_\mathbf{k}|^2\left(t-\frac{e^{-i\omega_k t}-1}{-i\omega_k}\right)}{i\omega_k}\sigma_z^{(n)}\sigma_z^{(m)}\right]. \end{aligned} \tag{A13}$$

When $[\hat{A},[\hat{A},\hat{B}]]=[\hat{B},[\hat{A},\hat{B}]]=0$, we have $e^{\hat{A}+\hat{B}}=e^{\hat{A}}e^{\hat{B}}e^{-[\hat{A},\hat{B}]/2}$. Applying this formula, we get

$$\begin{aligned} \exp\left[\int_0^t \hat{A}(t_1)dt_1\right]\exp\left[\int_0^t B(t_1)dt_1\right] &= \exp\left[\int_0^t A(t_1)+B(t_1)dt_1\right]\exp\left(\frac{1}{2}\int_0^t dt_1\int_0^t dt_2[A(t_1),B(t_2)]\right) \\ &= \exp\left[\int_0^t A(t_1)+B(t_1)dt_1\right]\exp\left(\sum_{n,m,\mathbf{k}}\frac{|g_\mathbf{k}|^2}{2{\omega_k}^2}(2-e^{i\omega_k t}-e^{-i\omega_k t})\sigma_z^{(n)}\sigma_z^{(m)}\right). \end{aligned} \tag{A14}$$

Substituting this into Eq. (A13), we finally get

$$U_I(t)=\exp\left[\int_0^t A(t_1)+B(t_1)dt_1\right]\exp\left[i\sum_{n,m,\mathbf{k}}\frac{|g_\mathbf{k}|^2\sigma_z^{(n)}\sigma_z^{(m)}}{{\omega_k}^2}(\omega_k t-\sin\omega_k t)\right], \tag{A15}$$

which proves Eq. (18).

2. Derivation of the reduced density operator of the qubits

In this section, we present the detailed calculation for Eq. (22). The density operator for the whole system is

$$\rho_I(t)=U_I(t)\rho_I^Q(0)\otimes\rho_I^B(0)U_I^\dagger(t), \tag{A16}$$

where the subscript I indicates the interaction picture, and the superscripts Q and B indicate qubits and the boson environment, respectively. What we really care about is the reduced density matrix of the qubits:

$$\rho_I^Q(t)=\mathrm{Tr}_B\left[U_I(t)\rho_I^Q(0)\otimes\rho_I^B(0){U_I}^\dagger(t)\right]. \tag{A17}$$

We now evaluate each matrix element of $\rho_I^Q(t)$. We define

$$\rho^Q_{I,\{i_n,j_n\}}(t)\equiv\langle i_1,i_2,\ldots,i_N|\rho_I^Q(t)|j_1,j_2,\ldots,j_n\rangle, \tag{A18}$$

where N is the total number of qubits, and $i_n=\pm1$ is the state of the nth qubit in the cluster state. We have

$$\rho^Q_{I,\{i_n,j_n\}}(t)=\mathrm{Tr}\left[\rho_I^B(0)U_I^{\dagger\{j_n\}}(t)U_I^{\{i_n\}}(t)\right]\rho^Q_{I,\{i_n,j_n\}}(0), \tag{A19}$$

where

$$U_I^{\{i_n\}}(t)=\exp\left[i\sum_{\mathbf{k}}|g_\mathbf{k}|^2 s(\omega_k,t)\sum_{n,m}i_n i_m\right]\exp\left\{\sum_{n,\mathbf{k}}[g_\mathbf{k}\varphi_{\omega_k}(t)i_n a_\mathbf{k}^\dagger-g_\mathbf{k}^*\varphi_{\omega_k}^*(t)i_n a_\mathbf{k}]\right\} \tag{A20}$$

satisfies

$$U_I(t)|\{i_n\}\rangle=U_I^{\{i_n\}}(t)|\{i_n\}\rangle. \tag{A21}$$

Explicit calculation reveals that

$$\begin{aligned} U_I^{\dagger\{j_n\}}(t)U_I^{\{i_n\}}(t) &= \exp\left[i\sum_{\mathbf{k}}|g_k|^2 s(\omega_k,t)\sum_{n,m}(i_n i_m-j_n j_m)\right]\exp\left[\sum_{n,\mathbf{k}}[g_\mathbf{k}^*\varphi_{\omega_k}^*(t)j_n a_\mathbf{k}-g_\mathbf{k}\varphi_{\omega_k}(t)j_n a_\mathbf{k}^\dagger]\right] \\ &\times\exp\left[\sum_{n,\mathbf{k}}[g_\mathbf{k}\varphi_{\omega_k}(t)i_n a_\mathbf{k}^\dagger-g_\mathbf{k}^*\varphi_{\omega_k}^*(t)i_n a_\mathbf{k}]\right] \end{aligned}$$

$$= \exp\left[i \sum_{\mathbf{k}} |g_k|^2 s(\omega_k,t) \sum_{n,m} (i_n i_m - j_n j_m) \right]$$

$$\times \exp\left[\sum_{n,\mathbf{k}} [g^*_{\mathbf{k}} \varphi^*_{\omega_k}(t)(j_n - i_n) a_{\mathbf{k}} - g_{\mathbf{k}} \varphi_{\omega_k}(t)(j_n - i_n) a^\dagger_{\mathbf{k}}] \right]. \tag{A22}$$

We here, again, use the fact that $e^{\hat{A}+\hat{B}} = e^{\hat{A}} e^{\hat{B}} e^{-[\hat{A},\hat{B}]/2}$ when $[\hat{A},[\hat{A},\hat{B}]] = [\hat{B},[\hat{A},\hat{B}]] = 0$. Substituting Eq. (15), the initial density operator of the boson environment, into it, we have

$$\mathrm{Tr}_B \left[\rho^B_I(0) \exp\left\{ \sum_{\mathbf{k}} (\phi_{\mathbf{k}} b^\dagger_{\mathbf{k}} - \phi^*_{\mathbf{k}} b_{\mathbf{k}}) \right\} \right] = \prod_{\mathbf{k}} \exp\left[-|g_{\mathbf{k}}|^2 \frac{1-\cos(\omega_k t)}{\omega_k^2} \coth\left(\frac{\omega_k}{2k_B T} \right) \sum_{m,n} (i_m - j_m)(i_n - j_n) \right], \tag{A23}$$

where

$$\phi_{\mathbf{k}} \equiv g_{\mathbf{k}} \phi_{\omega_k}(t) \sum_n (i_n - j_n). \tag{A24}$$

This equation leads to

$$\rho^Q_{I,\{i_n,j_n\}}(t) = \exp\left[- \sum_{\mathbf{k},m,n} |g_{\mathbf{k}}|^2 c(\omega_k,t) \coth\left(\frac{\omega_k}{2k_B T} \right) (i_m - j_m)(i_n - j_n) \right] \exp\left[i \sum_{\mathbf{k},m,n} |g_{\mathbf{k}}|^2 s(\omega_k,t)(i_m i_n - j_m j_n) \right] \rho^Q_{I,\{i_n,j_n\}}(0), \tag{A25}$$

where

$$c(\omega_k,t) = \frac{1-\cos(\omega_k t)}{{\omega_k}^2}. \tag{A26}$$

Taking the continuum limit, we get the form of Eq. (22), with

$$\Theta(t) = \int d\omega I(\omega) s(\omega,t), \tag{A27}$$

$$\Gamma(t,T) = \int d\omega I(\omega) c(\omega,t) \coth\left(\frac{\omega}{2\omega_T} \right). \tag{A28}$$

Here, $\omega_T \equiv k_B T$ is called the thermal frequency, and the spectral density

$$I(\omega) \equiv \sum_{\mathbf{k}} \delta(\omega - \omega_k) |g_{\mathbf{k}}|^2 \equiv \frac{dk}{d\omega} G(\omega) |g(\omega)|^2, \tag{A29}$$

with $G(\omega)$ being the density of states. Assuming an ohmic spectral density,

$$I(\omega) = \eta \omega e^{-\omega/\omega_c}, \tag{A30}$$

we get Eqs. (24) and (25).

[1] R. Raussendorf and H. J. Briegel, Phys. Rev. Lett. **86**, 5188 (2001).
[2] R. Raussendorf, D. E. Browne, and H. J. Briegel, Phys. Rev. A **68**, 022312 (2003).
[3] H. J. Briegel, D. E. Browne, W. Duer, R. Raussendorf, and M. Van den Nest, Nature Phys. **5**, 19 (2009).
[4] D. E. Browne and T. Rudolph, Phys. Rev. Lett. **95**, 010501 (2005).
[5] M. A. Nielsen, Phys. Rev. Lett. **93**, 040503 (2004).
[6] G.-P. Guo, H. Zhang, T. Tu, and G.-C. Guo, Phys. Rev. A **75**, 050301 (2007).
[7] S. D. Bartlett and T. Rudolph, Phys. Rev. A **74**, 040302 (2006).
[8] Y. Li, D. E. Browne, L. C. Kwek, R. Raussendorf, and T. C. Wei, Phys. Rev. Lett. **107**, 060501 (2011).
[9] P. Walther, K. J. Resch, T. Rudolph, E. Schenck, H. Weinfurter, V. Vedral, M. Aspelmeyer, and A. Zeilinger, Nature **434**, 169 (2005).
[10] K. Chen, C.-M. Li, Q. Zhang, Y.-A. Chen, A. Goebel, S. Chen, A. Mair, and J.-W. Pan, Phys. Rev. Lett. **99**, 120503 (2007).
[11] M. S. Tame, R. Prevedel, M. Paternostro, P. Bohi, M. S. Kim, and A. Zeilinger, Phys. Rev. Lett. **98**, 140501 (2007).
[12] C.-Y. Lu, X.-Q. Zhou, O. Guehne, W.-B. Gao, J. Zhang, Z.-S. Yuan, A. Goebel, T. Yang, and J.-W. Pan, Nature Phys. **3**, 91 (2007).
[13] R. Prevedel, A. Stefanov, P. Walther, and A. Zeilinger, New J. Phys. **9**, 205 (2007).
[14] Y. Tokunaga, S. Kuwashiro, T. Yamamoto, M. Koashi, and N. Imoto, Phys. Rev. Lett. **100**, 210501 (2008).

[15] W.-B. Gao, X.-C. Yao, J.-M. Cai, H. Lu, P. Xu, T. Yang, C.-Y. Lu, Y.-A. Chen, Z.-B. Chen, and J.-W. Pan, Nat. Photon. **5**, 117 (2011).
[16] Y. Tokunaga, T. Yamamoto, M. Koashi, and N. Imoto, Phys. Rev. A **74**, 020301 (2006).
[17] T. Yu and J. H. Eberly, Science **323**, 598 (2009).
[18] Y. S. Weinstein, Phys. Rev. A **79**, 052325 (2009).
[19] K. Fujii, Y. Nakata, M. Ohzeki, and M. Murao, Phys. Rev. Lett. **110**, 120502 (2013).
[20] M. Nielsen and I. Chuang, *Quantum Computation and Quantum Information* (Cambridge University Press, Cambridge, 2010), pp. 474–494.
[21] P. Jouzdani, E. Novais, and E. R. Mucciolo, Phys. Rev. A **88**, 012336 (2013).
[22] H. J. Briegel and R. Raussendorf, Phys. Rev. Lett. **86**, 910 (2001).
[23] D. Gottesman and I. L. Chuang, Nature **402**, 390 (1999).
[24] T. Chung, S. D. Bartlett, and A. C. Doherty, Can. J. Phys. **87**, 219 (2009).
[25] R. H. Dicke, Phys. Rev. **93**, 99 (1954).
[26] A. J. Leggett, S. Chakravarty, A. T. Dorsey, M. P. A. Fisher, A. Garg, and W. Zwerger, Rev. Mod. Phys. **59**, 1 (1987).
[27] P. Forn-Díaz, J. Lisenfeld, D. Marcos, J. J. García-Ripoll, E. Solano, C. J. P. M. Harmans, and J. E. Mooij, Phys. Rev. Lett. **105**, 237001 (2010).
[28] J. H. Reina, L. Quiroga, and N. F. Johnson, Phys. Rev. A **65**, 032326 (2002).
[29] L. G. E. Arruda, F. F. Fanchini, R. d. J. Napolitano, J. E. M. Hornos, and A. O. Caldeira, Phys. Rev. A **86**, 042326 (2012).
[30] G. Mahan, *Many-Particle Physics*, 3rd ed. (Springer-Verlag, New York, 2000), p. 240.